Grant agreement No: 101017008

Harmony

Assistive robots for healthcare

Enhancing Healthcare with Assistive Robotic Mobile Manipulation

(HARMONY) | H2020-ICT-2018-20| RIA

Start of the project: 01.01.2021
Duration: 42 months

Deliverable Number	
Deliverable Name	Compliant whole-body motion control
WP Number	7
Lead Beneficiary	CREATE
Dissemination Level	Public (PU)
Internal Reviewer	ABB
Due Date	31.12.2023
Date of Submission	
Version	2

This project has received funding from the European Union's Horizon 2020 research and innovation programme under grant agreement No 101017008

Revision History

Version	Date	Author(s)	Comments
1	01/12/2023	Fabio Ruggiero Mario Selvaggio Francesco Cufino	
2	29/12/2023	Fabio Amadio	Revised version

Table of Contents

1. Summary

This document describes the compliant whole-body motion control framework, focusing on its implementation on the mobile Yumi robot, which is the platform used to integrate the KUH and USZ use cases. After a brief review of the state of the art a compliant whole-body control architecture is presented in Section 2. This is followed by the jerk-based model-predictive controller proposed in Section 3 that allows realizing explicit feedback and control of the interaction forces. This work aims to make the robot able to solve mobile manipulation tasks by exploiting the system's redundancy while being compliant with external interactions. Indeed, the critical feature of a robot which works in a human-centred environment is safety, which is strictly related to system compliance.

2. Compliant whole-body control

2.1 State of the art

Compliant whole-body control consists of controlling an intrinsically redundant system exploiting the numerous degrees of freedom (DoFs) to simultaneously execute different prioritized tasks while being compliant with respect to external interactions.
Since the 1980s, researchers have delved into the issue of redundancy resolution, particularly in Cartesian space control of manipulators with more actuated DoFs than the task space dimension. The introduction of the null space projection, as pioneered by [1], [2], [3], offered a partial solution. This approach addressed redundancy by executing additional tasks in the null space of the end-effector task without interfering with its execution. Subsequently, various frameworks have evolved, building upon these fundamental techniques and incorporating enhancements in computational aspects [4], singularity-robustness [5], motion generation [6], and the extension to complex multi-priority hierarchies [7].

In the domain of whole-body control, attractive and repulsive artificial potential fields [8] have become prevalent for achieving tasks. Numerous solutions exist for specific control challenges, such as collision avoidance [9], [10], manipulator singularity avoidance [11], singularity avoidance for wheeled platforms [12], dual-arm manipulation [13], and joint limit avoidance [14]. Notably, since the early 2000s, there has been a surge in whole-body controllers simultaneously addressing multiple objectives facilitated by suitable simulation models and hardware availability. Influential work in multi-task hierarchies includes studies by Sentis et al. [15], [16] and Khatib et al. [17], [18], with subsequent implementations on real robots, such as the simulation on ASIMO by Hammam et al. [19] and application to a torque-controlled lightweight robot [20].
The application of these concepts to real robots is on the rise. Yoshikawa and Khatib [21] implemented an inverse model for soft contact behaviour on a position-controlled robot. At the same time, an open-source software package for whole-body compliance was introduced by Philippsen et al. [22] and utilized on robots like PR2 and Dreamer. Moro et al. [23] implemented an attractor-based multi-task method on the legged COMAN robot, and Nagasaka et al. [24] developed a whole-body algorithm for a 21-DoF wheeled system. However, certain aspects like singularity treatment and collision avoidance were not considered. Ott et al. [25] proposed a whole-body compliance controller for kinesthetic

teaching of torque-controlled robots, implemented on TORO, a legged humanoid based on DLR lightweight robot technology.
In [26], a way to design a compliant whole-body control is described exhaustively. A whole-body impedance control formulation has been treated, and stability analysis for arbitrarily complex multi-task hierarchies exploiting a priority-based dynamics representation has been addressed.

In summary, a suitable compliant whole-body control should be designed according to the following requirements:

- Safety features, task execution, and optimization criteria must be simultaneously achieved according to a particular priority;
- The order of priority has to be satisfied, and the task hierarchy must be flexible to manage unilateral constraints, dynamic modifications, and singularities;
- The stability of the closed loop must be ensured;
- The robot must physically interact with its environment in a compliant way so that no human in its workspace may come to harm.

The last requirement is the most important since, in our case, we need to define it as a system critical feature compliance.

2.2 Methods

2.2.1 Whole-body inverse kinematics

The mobile base of mobile Yumi is a four-wheeled nonholonomic base. For the overall motion, it has 3 DoFs: two for translations in the plane and one for rotation around its vertical axis. The base coordinates are denoted as $q_b \in \mathbb{R}^3$, with $q_b = [x_b \quad y_b \quad \theta_b]^T$. The mobile base is kinematically controlled: assuming that it is feedback linearizable, it is possible to send a desired velocity command $\dot{q}_{b_{des}}(t)$ and to suppose that $\dot{q}_{b_{des}}(t) \approx \dot{q}_b(t)$.
For what concerns the upper body, mobile Yumi has two 7-DoF redundant arms whose coordinates are denoted with $q_r, q_l \in \mathbb{R}^7$, respectively, for right and left arm, and 1-DoF at the torso denoted with $q_t \in \mathbb{R}$. Stacking the vectors, we obtain the generalized joint configuration vector $q \in \mathbb{R}^n$, with $q = [q_b^T \quad q_r^T \quad q_l^T \quad q_t^T]^T$, $n = n_b + 3$, $n_b = 15$.
The adopted method to solve the tasks consists of planning a trajectory in the task space (for the single right or left arm, or both) and solving the whole-body inverse kinematics to get the correspondent generalized joint variables provided to an impedance controller.
Consider a task described by

$$x = f(q),$$

where $x \in \mathbb{R}^m$ represents the task coordinates, with $m \leq n$, and $f: \mathbb{R}^n \to \mathbb{R}^m$ is the task function. The differential mapping from the generalized joint velocities to task velocities is determined by the Jacobian $J(q) \in \mathbb{R}^{m \times n}$

$$\dot{x} = J(q)\dot{q}.$$

The desired task space trajectory is provided in terms of position, velocity and acceleration $x_{des}(t), \dot{x}_{des}(t), \ddot{x}_{des}(t)$ and an inverse kinematics is performed through hierarchical quadratic programming, as shown in [27,32], giving as output the correspondent quantities in terms of generalized joint variables $q_{des}(t), \dot{q}_{des}(t), \ddot{q}_{des}(t)$. These references are provided to an impedance controller which generates the torques for this task.

2.2.2 Admittance interface to the mobile base

A force-torque interface for the mobile base is introduced before describing the impedance controller that generates the task's torques. That is because, in this way, it is possible to design a whole-body impedance controller computing simultaneously the torques for the arms and the virtual torques for the mobile base. Then, this interface maps the virtual torques into the mobile base velocity. To this goal, an admittance with virtual platform inertia and virtual damping is simulated as

$$M_{adm}\ddot{q}_b + D_{adm}\dot{q}_b = \tau_{b,virt} + \tau_{b,ext}\,,$$

where $M_{adm}, D_{adm} \in \mathbb{R}^{3\times3}$ are the virtual inertia and damping, respectively, $\tau_{b,virt}, \tau_{b,ext} \in \mathbb{R}^3$ are the virtual torques input and the external torques, respectively. If $\tau_{b,ext}$ is not available, it can be set to zero.

2.2.3 Impedance control

Whole-body dynamics

Consider the whole-body dynamics obtained adding the mobile base admittance interface to the upper body dynamics

$$B(q)\ddot{q} + C(q,\dot{q})\dot{q} + g(q) + F\dot{q} = u - \tau_{ext}.$$

The terms in the equation are the following.

- $B(q) = \begin{bmatrix} M_{adm} & O \\ M_{qb} & M_{qq} \end{bmatrix} \in \mathbb{R}^{n\times n}$ denotes the generalized inertia matrix of the robot, with $M_{qq} \in \mathbb{R}^{n_b\times n_b}$ the upper body inertia matrix, and $M_{qb} \in \mathbb{R}^{n_b\times 3}$ the inertia coupling to mobile base;
- $C(q,\dot{q}) = \begin{bmatrix} D_{adm} & O \\ C_{qb} & C_{qq} \end{bmatrix} \in \mathbb{R}^{n\times n}$ denotes the generalized Coriolis/centrifugal terms of the robot, with $C_{qq} \in \mathbb{R}^{n_b\times n_b}$ the upper body ones, and $C_{qb} \in \mathbb{R}^{n_b\times 3}$ the coupling to mobile base ones;
- $g(q) = \begin{bmatrix} 0 \\ g_q \end{bmatrix} \in \mathbb{R}^n$ denotes the generalized gravity, $g_q \in \mathbb{R}^{n_b}$ is the upper body gravity;
- $F = \begin{bmatrix} O & O \\ O & F_q \end{bmatrix} \in \mathbb{R}^{n\times n}$ comprises either the sliding or rolling friction matrix for upper body;
- $u = \begin{bmatrix} \tau_{b,virt} \\ \tau_q \end{bmatrix} \in \mathbb{R}^n$ is the control input vector, with $\tau_q \in \mathbb{R}^{n_b}$ input torques for upper body;
- $\tau_{ext} = \begin{bmatrix} \tau_{b,ext} \\ \tau_{q,ext} \end{bmatrix} \in \mathbb{R}^n$ denotes the external torques, with $\tau_{q,ext} \in \mathbb{R}^{n_b}$ external upper body torques.

Mobile base and upper body decoupling

Before proceeding, it is necessary to get rid of the coupling terms M_{qb} and C_{qb}. To do that, the control input is chosen as

$$u = u_{imp} + u_{comp}$$

with

$$u_{comp} = \begin{bmatrix} 0 \\ M_{qb}\ddot{q}_b + C_{qb}\dot{q}_b \end{bmatrix}$$

where the base accelerations can be obtained as

$$\ddot{q}_b = M_{adm}^{-1}\left(\tau_{b,virt} + \tau_{b,ext} - D_{adm}\dot{q}_b\right).$$

With this choice, the dynamics becomes the following (the dependencies are omitted for ease of readability)

$$\underline{B}\ddot{q} + \underline{C}\dot{q} + g + F\dot{q} = u_{imp} - \tau_{ext},$$

with $\underline{B} = \begin{bmatrix} M_{adm} & O \\ O & M_{qq} \end{bmatrix} \in \mathbb{R}^{n\times n}$ and $\underline{C} = \begin{bmatrix} D_{adm} & O \\ O & C_{qq} \end{bmatrix} \in \mathbb{R}^{n\times n}$.

Impedance control design

With this formulation, we could define the u_{imp} basing on a virtual potential representing a spatial spring in Cartesian space, avoiding considering the whole-body inverse kinematics

$$V_{imp}\left(\tilde{x}(q)\right) = \frac{1}{2}\tilde{x}^T(q)K\tilde{x}(q),$$

with $\tilde{x} \in \mathbb{R}^6$ error in Cartesian space and $K \in \mathbb{R}^{6\times6}, K > 0$. In this case, the control input would be

$$u_{imp} = -\left(\frac{\partial V_{imp}\left(\tilde{x}(q)\right)}{\partial q}\right)^T,$$

adding then a further damping injection.

However, for our application, a classical joint impedance control (keeping the whole-body inverse kinematics) has been preferred, since the presence of significant unmodeled friction prevents the deployment of a Cartesian impedance control.

We can design the impedance control for the upper body since the mobile base already has the desired virtual damping and stiffness designed for the admittance interface. Let $q_q \in \mathbb{R}^{n_b}$ **be** the upper body coordinates. Upper body equation is (dependencies are omitted)

$$M_{qq}\ddot{q}_q + C_{qq}\dot{q}_q + g_q + F_q\dot{q}_q = \tau_q - \tau_{q,ext}.$$

Encompass all the nonlinearities in the model in the following term

$$n = C_{qq}\dot{q}_q + g_q + F_q\dot{q}_q.$$

Then, the upper body dynamics so becomes

$$M_{qq}\ddot{q}_q + n = \tau_q - \tau_{q,ext}.$$

Supposing that we can measure the external torques, choose the input torques to linearize the system as

$$\tau_q = M_{qq} y + n + \tau_{q,ext}.$$

The vector $y \in \mathbb{R}^{n_b}$ is an auxiliary control. With this choice, the dynamics becomes

$$M_{qq} \ddot{q}_q = M_{qq} y.$$

The auxiliar control is chosen to realize a desired mechanical impedance in joint space, with a desired inertia $M_d \in \mathbb{R}^{n_b \times n_b}$, damping $D_d \in \mathbb{R}^{n_b \times n_b}$, and stiffness $K_d \in \mathbb{R}^{n_b \times n_b}$. To this goal, the external torques are also injected into the system as

$$y = M_d^{-1}\left(M_d \ddot{q}_{q_d} + D_d \dot{\tilde{q}} + K_d \tilde{q} - \tau_{q,ext}\right).$$

The quantity $q_{q_d} \in \mathbb{R}^{n_b}$ is the reference obtained from inverse kinematics, and $\tilde{q} = q_{q_d} - q$ is the tracking error.
Substituting, the closed loop dynamics is

$$M_d \ddot{\tilde{q}} + D_d \dot{\tilde{q}} + K_d \tilde{q} = \tau_{q,ext}.$$

Finally, the system represents a fully decoupled and linear spring-mass-damper model when interacting with the environment. However, to get this behavior, we need to measure $\tau_{q,ext}$. If this measure is not available, we can repeat the same passages by considering $\tau_{q,ext} = 0$ in control laws. This leads to the following closed-loop dynamics

$$M_d \ddot{\tilde{q}} + D_d \dot{\tilde{q}} + K_d \tilde{q} = M_d M_{qq}^{-1} \tau_{q,ext}.$$

To remove the coupling through inertia matrix, we can choose the real inertia of the upper body $M_d = M_{qq}$ and obtain

$$M_{qq} \ddot{\tilde{q}} + D_d \dot{\tilde{q}} + K_d \tilde{q} = \tau_{q,ext}.$$

2.2.4 Task hierarchy and null space projections

Consider now *r* tasks described by

$$x_i = f_i(q), \qquad i \in [1, r],$$

where $x_i \in \mathbb{R}^{m_i}$ represents the i-th task coordinates and $f: \mathbb{R}^n \to \mathbb{R}^{m_i}$ is the i-th task function. The differential mapping for each task is

$$\dot{x}_i = J_i(q)\dot{q}, \qquad i \in [1, r],$$

where it is assumed that $J_i(q)$ is full rank $\forall i$. Suppose that the main task ($i = 1$) has dimension $m_1 < n$. Hence, a kinematic redundancy of $n - m_1$ DoFs remains to execute subtasks in its null space. The hierarchy is defined such that $i = 1$ is referred to as top priority and $i_a < i_b$ implies that i_a has higher priority than i_b. If a minor priority task is projected into the null space of a major priority task, this does not affect the major priority one. Then, we can implement the task hierarchy through successive projection of the torques as following

$$\tau_i^p = N_i(q)\tau_i \qquad i \in [2, r],$$

with

$$N_i(q) = N_{i-1}(q)(I - J_{i-1}^T(q)(J_{i-1}(q)^{W\dagger})^T).$$

The matrix $J_{i-1}(q)^{W\dagger} = W^{-1}J_{i-1}(q)^T(J_{i-1}(q)W^{-1}J_{i-1}(q)^T)^{-1}$ is the weighted pseudoinverse. It is shown that choosing $W = I$ guarantees static consistency, while $W = M_{qq}$ leads to dynamic consistency [28].

The total control torque is obtained by summing the main task torque and all the projected ones

$$\tau = \tau_1 + \sum_{i=2}^{r} \tau_i^p.$$

The task torques are usually chosen using artificial potentials for obstacle avoidance, singularity avoidance (safety), manipulability maximization (performance) and so on. Of course, safety tasks have always been a greater priority than performance ones.

3. Jerk-based Model-Predictive Control

In the previous section, we have overviewed a general torque-based whole-body control architecture to realize compliant interaction of the robot with the environment. Here, we extend the previous architecture by developing an optimal controller with model-based prediction capabilities. This is conceived to render control torques continuous while allowing control by direct feedback of the contact forces.

3.1 Task hierarchy and null space projections

Model-predictive control (MPC) is a well-established control framework for general dynamical systems. It has been used in robotics for many applications. In robot manipulation, the current trend is to develop control frameworks that integrate contact forces tracking as an objective and feedback on their measure in the controller [30]. In this way, the controller directly computes the actuation torques to exert desired forces on the environment and realize contact forces between the hand and the object that satisfy friction cone constraints, thus enforcing a non-sliding behavior. This framework can be used to enforce the desired compliant behavior of the robot with respect to the environment by direct feedback of the contact force measurements, as discussed in the following.

To guarantee a continuous execution of the task, jerk control is used. This considers the rate-of-change of the joint torques as the output of the controller, which, once integrated over time, returns the torque input of our robotic system [31]. This procedure makes the obtained joint torque profile (and thus the system accelerations) continuous and allows the integration of force signals stemming from the interaction as feedback into the controller. This is achieved by considering an extended state vector that reads as $x = [\tau^T \quad q^T \quad \dot{q}^T \quad \Lambda^T]^T$ where τ is the control torque of the manipulator, q and $\dot{q}$ joint values and their time derivative, and Λ is the vector of coefficients that are used to parametrized contact forces (see later). With this choice, we increase the relative degree of our system dynamics and choose as a control input $u = \dot{\tau}$. With the state/input choice made, the continuous-time dynamic evolution of the extended state can be written as

$$\dot{x} = f(x,u) = \begin{cases} \dot{\tau} = u \\ \dot{q} = \dot{q} \\ \ddot{q} = \tilde{M}^{-1}(x)(\tau - \tilde{C}(x)\dot{q} - \tilde{n}(x)) \\ \dot{\Lambda} = \left(G\hat{F}_c\right)^{\dagger}\left(A\dot{\tau} + B\tau + C\right) \end{cases}$$

where the matrices A, B, and C write as follows:

$$A = M_o J \tilde{M}^{-1}, \quad B = M_o \dot{J} \tilde{M}^{-1}, \; C = -2M_o \dot{J} \tilde{M}^{-1} \tilde{n}.$$

In the above equations, the following combined robot/object dynamic model is used

$$\tilde{M}(q)\ddot{q} + \tilde{C}(q,\dot{q})\dot{q} + \tilde{n}(q,\dot{q}) = \tau$$

This is retrieved from the manipulator and object dynamical models considering persistent contacts between them. Note that this is not an assumption as relative sliding is prevented by our controller. The matrices involved in the above equation can be explicitly defined as

$$\begin{aligned} \tilde{M} &= M_m + J_o^{\mathrm{T}} M_o J_o \\ \tilde{C} &= C_m + J_o^{\mathrm{T}}\left(C_o J_o + M_o \dot{J}_o\right) \\ \tilde{n} &= n_m + J_o^{\mathrm{T}} n_o. \end{aligned}$$

where $M_m(q) \in \mathbb{R}^{n\times n}$ is the symmetric positive-definite robot joint-space inertia matrix, $C_m(q,\dot{q}) \in \mathbb{R}^{n\times n}$ is the matrix of centrifugal/Coriolis terms, $n_m(q) \in \mathbb{R}^n$ is the gravity vector, $\tau \in \mathbb{R}^n$ is the vector of joint torques (representing the overall control input of the robotic system), and $M_o(x_o) \in \mathbb{R}^{6\times 6}$ is the object positive-definite mass/inertia matrix, $C_o(q,\dot{q}) \in \mathbb{R}^{6\times 6}$ is the matrix of centrifugal/Coriolis terms, $n_o(q) \in \mathbb{R}^6$ is the gravity vector, and $J_o \in \mathbb{R}^{6\times n}$ is the object geometric Jacobian matrix.

The optimization problem that realize the devised nonlinear MPC controller is (in discrete time)

$$\begin{aligned} &\min_{x,u} \|x_e^* - x_e\|_{Q_e}^2 + \sum_{i=0}^{N-1} \|x_{i+1}^* - x_{i+1}\|_{Q_i}^2 + \|u_i\|_{R_i}^2 \\ &\text{s.t. } x_0 = \bar{x}(0) \\ &\quad x_{i+1} = f_k(x_i, u_i) \\ &\quad \underline{x} \le x_i \le \bar{x} \\ &\quad \underline{u} \le u_i \le \bar{u} \end{aligned}$$

where Q and R matrices are weights, x^* are reference values, the last two equations represent bounds on input/state. The non-sliding constraint is encoded in this as explained in the following section.

3.2 Object-manipulator interaction model

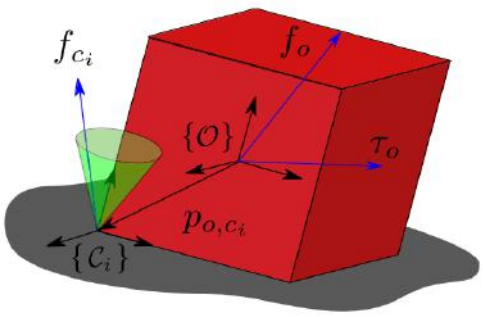

With reference to the above figure, the object body wrench $F_o = \begin{bmatrix} f_o{}^T & \tau_o^T \end{bmatrix}^T$ can be realized by opportunely generating contact forces $F_c = [\cdots \quad f_{ci}^T \quad \cdots]^T$ between the object and its manipulandum. We assume that the object's shape and dynamical properties are known and

coincident with a cuboid of known material. Moreover, we assume that the overall contact surface between the cuboid object and the tray can be approximated by discretizing it, i.e., using a finite number of n_c contact points located in the vertices of the object in contact (thus $n_c = 4$ in the considered case). The i-th contact point is thus identified by a contact frame $\{C_i\}$ whose pose is known and expressed in $\{O\}$ by $q_{o,ci} = [p_{o,ci}, R_{o,ci}] \in SE(3)$. Assuming a point contact with friction model, only the linear forces $f_{ci} \in \mathbb{R}^3$ can be transmitted through the i-th contact. The body wrench F_o can thus be expressed as $F_o = GF$c, where $G \in \mathbb{R}^{6\times 3n_c}$, usually referred to as the *grasp matrix* in the robotic grasping literature.
To enforce the nonsliding constraint in the controller, it is convenient to parametrize the contact forces and make the constraint linear in the chosen parameters, i.e.

$$F_c = \hat{F}_c \Lambda$$

while Λ denotes the vector of contact force parameters that constitutes the components along the friction cone borders and $\hat{F}_c$ is the matrix describing the friction cone space geometry, as its columns contain the vectors of the friction cone edges, which are depicted in the following pictures

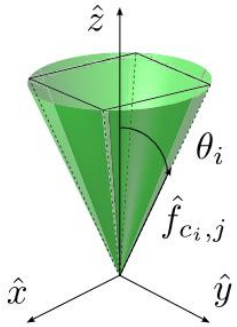

At this point, for Fc to belong to the approximated friction cone space, it is sufficient to choose

$$\Lambda_i \geq 0 \quad \forall\, i = 1, \ldots, kn_c$$

meaning that F_c must be a non-negative linear combination of the friction cone boundaries through the vector of the coefficients Λ.

4. Non-prehensile and bimanual manipulation

In the framework of compliant whole-body control, non-prehensile manipulation and bimanual manipulation tasks have been inserted to accomplish the requirements of the KUH use case, in which the robot must open a box and extract the racks.
It has been decided to integrate non-prehensile and bimanual manipulation in the compliant whole-body framework to realize a more flexible solution for the case study, considering that the box might arrive at the workstation with an unknown position and orientation. The robot and the box must be aligned appropriately to make the box opening feasible. Hence, it is necessary to manipulate the box before opening it. To this purpose, a realignment of the box has been tested and placed in the workflow before the box opening. For the realignment, four different cases have been experimented:

- non-prehensile clockwise reorientation with the right arm;
- non-prehensile counter-clockwise reorientation with the right arm;
- bimanual clockwise reorientation;

- bimanual counter-clockwise reorientation.

Furthermore, a bimanual non-prehensile box pushing has been tested to remove the box from the workstation. This was placed at the workflow's end after the box was emptied and closed. This work has been done using the already available planner and the compliant whole-body motion control developed on the mobile Yumi. In reorientation experiments, the box was full (the box contained four racks filled with test tubes), while in the pushing experiment, it was empty.

Moreover, we started devising a controller to endow the mobile Yumi platform with the capability to transport the objects extracted from the box around. The whole-body non-prehensile manipulation controller devised for this task relies on a jerk-based model-predictive control framework (see Section 3), and it has been preliminarily tested on the Rodyman humanoid robot. The controller assumes transporting a cuboid object in a fixed position on a tray-like end-effector. The object's initial position in the tray is preliminarily retrieved using an INTEL D415 vision sensor tracking a QR code through the VISP library. The goal was to control robot movements to avoid sliding the object along the performed transportation trajectory exploiting frictional contacts. Moreover, the controller enforces system constraints such as joint limits, velocities, and torques. The following section briefly presents the results achieved in this task. A deeper discussion about the controller performance achieved so far is shown in [29].

4.1 Non-prehensile clockwise (counterclockwise) reorientation with right arm

Non-prehensile clockwise (counter-clockwise) reorientation is needed if the angle describing the rotation around the z-axis of the box with respect to the robot base exceeds a certain positive (negative) threshold. The reorientation routine consists of positioning the arm wrist at the lower (upper) part of the right side of the box, with an orientation such that the wrist's flat surface and the box's face are parallel. Then, a setpoint along the entering normal direction to the box face is provided. After that, the procedure is iterated until the absolute value of rotation around the vertical axis is under the threshold. In that case, the task ends.

A test for each case (clockwise and counter-clockwise reorientation) has been done, starting with the box's initial orientation absolute value over the threshold. For each test, two iterations of the routine have been executed. Table 1 reports the rotation around z (ϑ coordinate) and the box frame's translation (x, y coordinates). The coordinates are referred with respect to a frame oriented as the base link frame and with the origin coincident with the initial box frame one to understand the orientation and translation variation quickly.

	Iteration	x [m]	y [m]	ϑ [deg]
Clockwise reorientation	**0**	0	0	29.7°
	1	−0.044	0.085	12.4°
	2	−0.063	0.165	−3.31°
	0	0	0	−29.7°

Counter-clockwise reorientation	**1**	0.037	0.064	$-17.9°$
	2	0.061	0.146	$-6.03°$

Table 1. Results of non-prehensile reorientation with right arm experiments

In the following set of pictures, it is possible to appreciate the non-prehensile clockwise reorientation with the right arm of the mobile Yumi platform.

In the following set of pictures, instead, it is possible to appreciate the non-prehensile counter-clockwise reorientation with the right arm of the mobile Yumi platform.

4.2 Bimanual clockwise (counter-clockwise) reorientation

Like the previous case, the clockwise (counter-clockwise) reorientation consists of positioning the right arm wrist at the lower (upper) part of the right side of the box, oriented as described in 4.1. At the same time, the left arm wrist is positioned at the upper (lower) part of the left side, oriented according to the same criterion. Then, like before, a setpoint along the entering normal direction to the box face is provided to the right arm, while the left one keeps its position, acting as a fulcrum. Again, the procedure is iterated until the absolute value of rotation around the vertical axis is under the threshold.

A test for each case (clockwise and counter-clockwise reorientation) has been done, and the results are reported in Table 2 according to the same convention described in Section 4.1. From the results, it is possible to observe that the reorientation objective (0°) is achieved with an acceptable error in each case. However, in this case of bimanual reorientation, the box translates less than in the single-arm case.

	Iteration	x [m]	y [m]	ϑ [deg]
Clockwise reorientation	**0**	0	0	32.9°
	1	−0.040	0.045	13.7°
	2	−0.061	0.091	−1.09°
Counter-clockwise reorientation	**0**	0	0	−31.6°
	1	0.024	0.024	−19.9°
	2	0.047	0.044	−9.22°

Table 2. Results of non-prehensile reorientation with the bimanual system

In the following set of pictures, it is possible to appreciate the non-prehensile clockwise reorientation with both arms of the mobile Yumi platform.


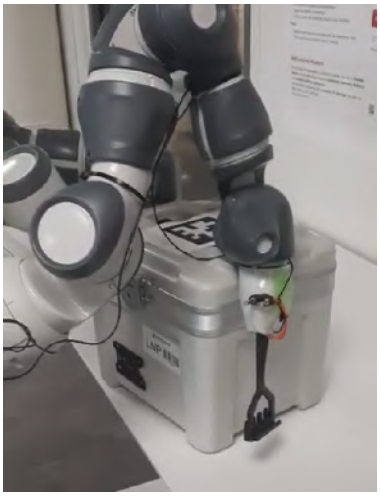


In the following set of pictures, it is possible to appreciate the non-prehensile counter-clockwise reorientation with both arms of the mobile Yumi platform.

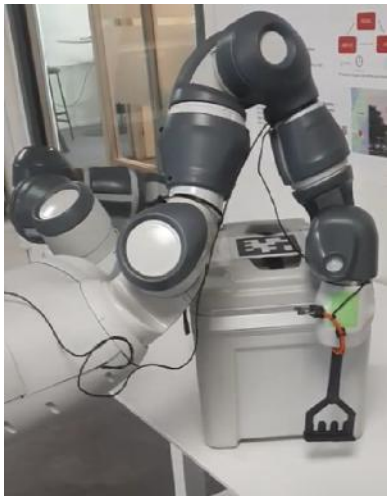

4.3 Non-prehensile pushing

Bimanual non-prehensile box pushing is needed to get it back to the work chain when the box is emptied. It consists in positioning both the arm wrists symmetrically in front of the box side facing the robot. Their orientation is such that the flat surface of the wrists and the face of the box are parallel. Then, two setpoints along the direction normal to the box face are provided to the arms.

A pushing test has been done to move the box outside from the workstation. The results are reported in Table 3, again with the convention described in Section 4.1. From the achieved results, it is possible to observe that the box is pushed away along x; y and ϑ are not subject to significant changes.

	Iteration	x [m]	y [m]	ϑ [deg]
Non-prehensile pushing	**0**	0	0	0.5°
	1	0.210	0.011	0.9°

Table 3. Results of non-prehensile pushing

In the following pictures, it is possible to appreciate the non-prehensile pushing action.


4.4 Non-prehensile tray-based object transportation

The results achieved using the model-predictive nonprehensile manipulation controller that avoids object sliding are reported in this section. The experimental setup is the Rodyman humanoid robot whose joint limits are reported in the table below.

REAL ROBOTIC SYSTEM JOINT LIMITS

Joint #	1	2	3	4	5	6	7	8	9
q [deg]	±170	±120	±120	±170	±120	±170	±170	±170	±170
$\dot{q}$ [deg/s]	±57	±57	±57	±57	±57	±57	±57	±57	±57
τ [Nm]	±176	±176	±110	±110	±110	±40	±40	±40	±40

It is a 21-DoF robot made of a custom-built mobile base, a two-DoFs torso, two one-Dof shoulders, and two six-DoFs Shunk Powerball arms. A plastic tray-like end-effector was attached to it through a 3-D printed support, which embedded a Shunk 6-Axis F/T sensor. A calibrated Intel RealSense Depth Camera D415 was mounted on the tray with the purpose of tracking and recording the object displacement thanks to a QR-code pattern and the VISP auto tracker module. The object is a steel hollowed cuboid of dimensions 60 × 60 × 70 mm whose inertial properties are: mass $m_o = 0.236$ kg and diagonal inertial matrix, $I_o = diag(4.5375 \cdot 10^{-5})$ kgm^2. The friction coefficient between the object and the tray has been experimentally identified in μ = 0.2. The robot was position-controlled, and its set point was extracted from the output trajectory solution of the devised controller.

The considered trajectories are shown in the figures below.

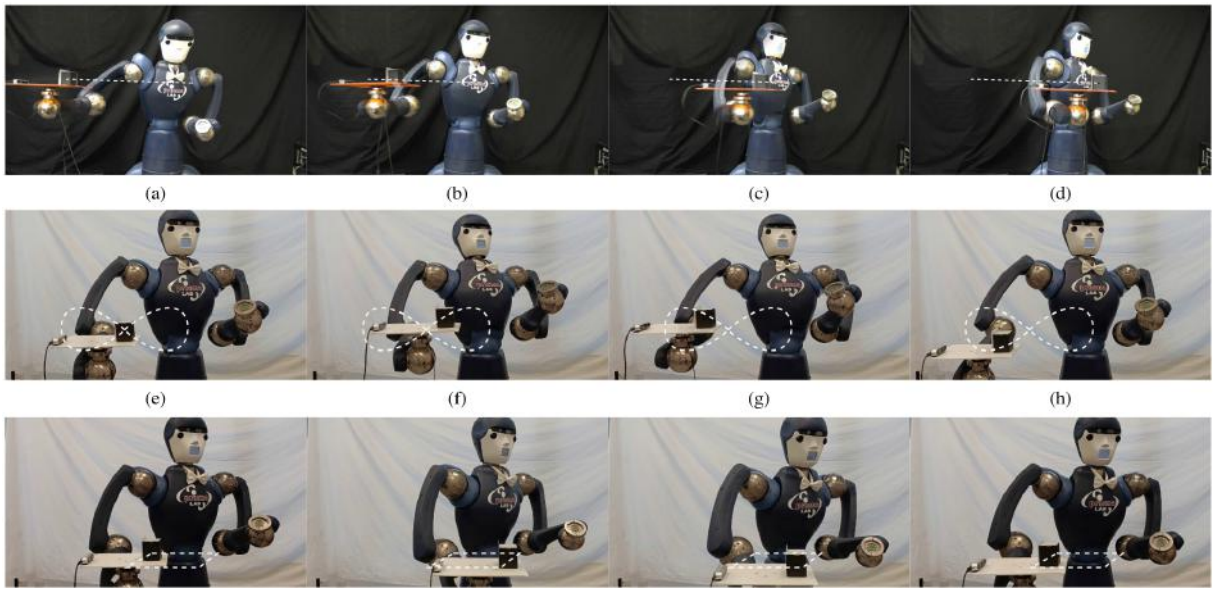

The first object trajectory chosen for the real experiment is a quintic polynomial rest-to-rest linear Cartesian trajectory with initial point $p_i = [0.7, -0.5, 1.34]$ m, and final point $p_e = [0.7, 0.15, 1.34]$ m expressed in the robot base frame, whose duration is $T = 1.5$ s. The desired orientation is kept constant and corresponding to the tray facing the upward direction. To additionally prove the robustness of our controller we consider two additional trajectories: a rectangular path in the horizontal plane and a Lemniscate-like path in the vertical plane.

The validation of the performance using the proposed controller onto the Rodyman robot is shown in the graphs below where $E = (e_p, e_o)$ is the position/orientation error, and D is the norm of the object displacement from its initial position.

.

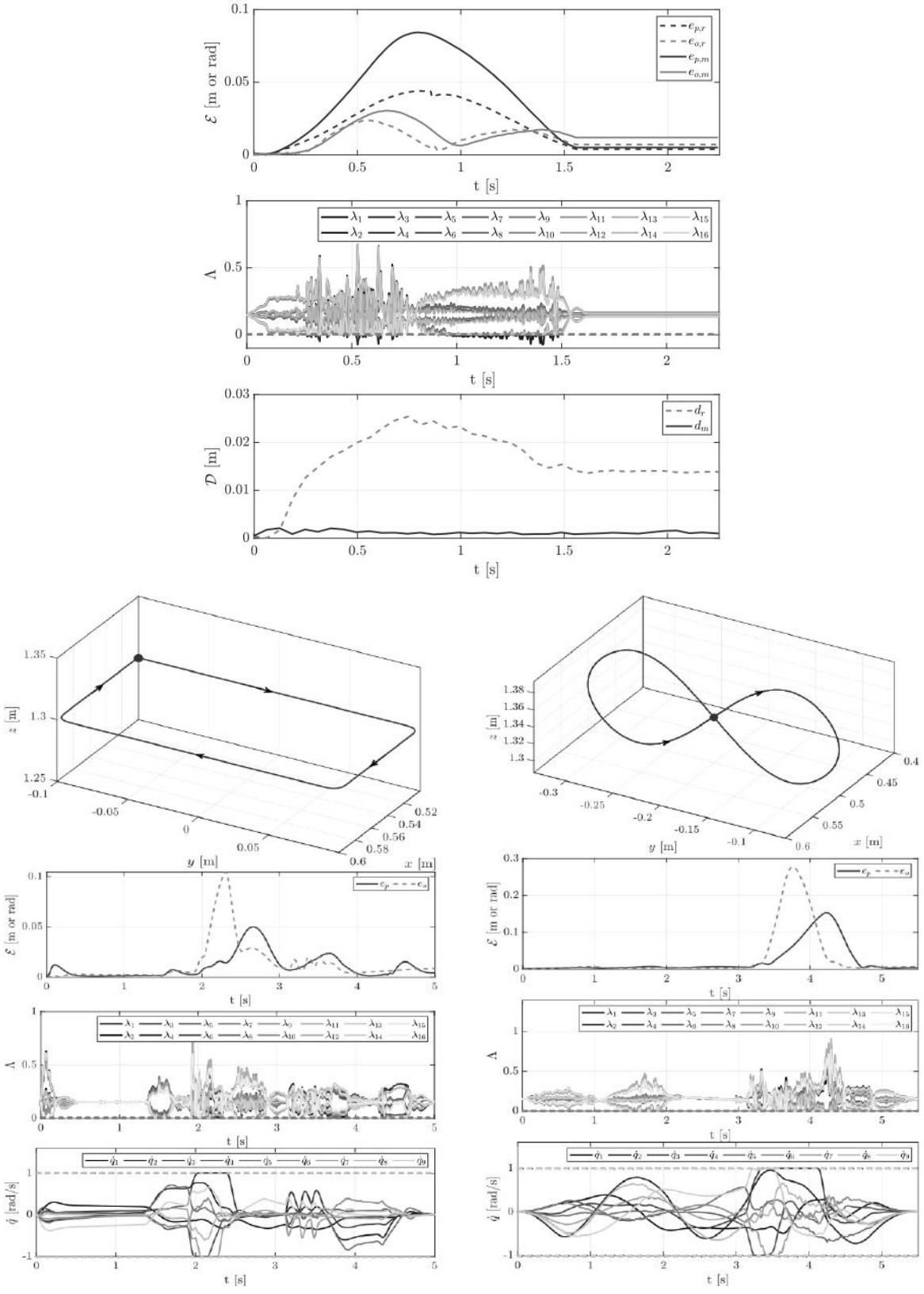

The results above demonstrate the capability of explicitly controlling contact forces exchanged by the manipulator with an environment (in this case, with the manipulated object). This is crucial for realizing a compliant behavior with desired impedance characteristics. Indeed, by using computed torques as a reference and opportunely modulating the controller gains, the robot's behavior can be made more or less stiff with respect to external interactions. It is worth noting that this capability can also be enabled by setting the robot already in joint compliant mode (as explained in Sec. 2) and setting the desired joint positions/velocities (computed from the controller in Sec. 3) as reference. This last choice would constitute a solution enhanced in terms of modularity.

5. Conclusion

In conclusion, a compliant whole-body control has been developed for the Mobile Yumi platform, making the robot able to solve various kinds of tasks simultaneously while being compliant with respect to any external interaction. The safety requirements are always the most fundamental, especially in our case, where the system has to work in an environment shared with humans. The non-prehensile and bimanual manipulation integrated into the whole-body framework is effectively executed in a compliant way, thus realizing the possibility of collaborating with a human operator. The same considerations can be drawn for the nonprehensile manipulation task, where compliance can be achieved by opportunely modulating the gains of the proposed jerk-based model predictive architecture and using the computed torques as input for the robotic system. Although the controllers have been developed as alternative solutions, we aim to integrate the two shortly and demonstrate the controllers' versatility and the framework's modularity.

References

[1] J. Baillieul, John M. Hollerbach, and Roger Brockett. “Programming and control of kinematically redundant manipulators”. In *Proc. of the 23rd IEEE Conference on Decision and Control*, pages 768–774, December 1984.

[2] Y. Nakamura, H. Hanafusa, and T. Yoshikawa. “Task-Priority Based Redundancy Control of Robot Manipulators”. *International Journal of Robotics Research* 6(2):3–15, June 1987.

[3] J. H. Hollerbach and K. Suh. “Redundancy Resolution of Manipulators through Torque Optimization”. *IEEE Journal of Robotics andAutomation*,RA-3(4):308–316, August 1987.

[4] P. Baerlocher and R. Boulic. Task-Priority Formulations for the Kinematic Control of Highly Redundant Articulated Structures. In *Proc. of the 1998 IEEE/RSJ International Conference on Intelligent Robots and Systems*, pages 323–329, October 1998.

[5] Y. Nakamura and H. Hanafusa. “Inverse Kinematic Solutions With Singularity Robustness for Robot Manipulator Control”. *Journal of Dynamic Systems, Measurement, and Control*, 108(3):163–171, September 1986.

[6] O. Brock, and O. Khatib. “Elastic Strips: A Framework for Motion Generation in Human Environments”. *International Journal of Robotics Research* 21(12):1031–1052, December 2002.

[7] B. Siciliano and J. Slotine. “A General Framework for Managing Multiple Tasks in Highly Redundant Robotic Systems”. In *Proc. of the 5th International Conference on Advanced Robotics*, pages 1211–1216, June 1991.

[8] O. Khatib. “Real-Time Obstacle Avoidance for Manipulators and Mobile Robots”. *International Journal of Robotics Research*, 5(1):90–98, Spring 1986.

[9] H. Sugiura, M. Gienger, H. Janssen, and C. Goerick. “Reactive Self Collision Avoidance with Dynamic Task Prioritization for Humanoid Robots”. *International Journal of Humanoid Robotics*, 7(1):31–54, 2010.

[10] A. De Santis, A. Albu-Schäffer, C. Ott, B. Siciliano, and G. Hirzinger. “The skeleton algorithm for self-collision avoidance of a humanoid manipulator.” In *Proc. of the 2007 IEEE/ASME International Conference on Advanced Intelligent Mechatronics*, September 2007.

[11] C. Ott. “Cartesian Impedance Control of Redundant and Flexible-Joint Robots”. *Springer Tracts in Advanced Robotics*, vol. 49. Springer Publishing Company, Berlin Heidelberg, 200.

[12] C. P. Connette, C. Parlitz, M. Hägele, and A. Verl. “Singularity Avoidance for Over-Actuated, Pseudo-Omnidirectional, Wheeled Mobile Robots”. In *Proc. of the 2009 IEEE International Conference on Robotics and Automation*, pages 4124–4130, May 2009.

[13] T. Wimböck, C. Ott, and G. Hirzinger. “Impedance Behaviors for Two-handed Manipulation: Design and Experiments”. In *Proc. of the 2007 IEEE International Conference on Robotics and Automation*, pages 4182–4189, April 2007.

[14] É. Marchand, F. Chaumette, and A. Rizzo. “Using the task function approach to avoid robot joint limits and kinematic singularities in visual servoing”. In *Proc. of the 1996 IEEE/RSJ International Conference on Intelligent Robots and Systems*, pages 1083–1090, November 1996.

[15] L. Sentis and O. Khatib. “Synthesis of Whole-Body Behaviors through Hierarchical Control of Behavioral Primitives”. *International Journal of Humanoid Robotics*, 2(4):505–518, January 2005.

[16] L. Sentis, J. Park, and O. Khatib. “Compliant Control of Multicontact and Center-of-Mass Behavior in Humanoid Robots”. *IEEE Transactions on Robotics* 26(3):483–501, June 2010.

[17] O. Khatib, L. Sentis, J. Park, and J. Warren. “Whole-Body Dynamic Behavior and Control of Human-like Robots”. *International Journal of Humanoid Robotics*, 1(1):29–43, March 2004.

[18] O. Khatib, L. Sentis, and J. Park. “A Unified Framework for Whole-Body Humanoid Robot Control with Multiple Constraints and Contacts.” In *European Robotics Symposium 2008*, pages 303–312, March 2008.

[19] G. B. Hammam, D. E. Orin, and B. Dariush. “Whole-Body Humanoid Control from Upper-Body Task Specifications”. In *Proc. of the 2010 IEEE International Conference on Robotics and Automation*, pages 3398–3405, May 2010.

[20] H. Sadeghian, L. Villani, M. Keshmiri, and B. Siciliano. “Dynamic multi-priority control in redundant robotic systems”. *Robotica*, 31(7):1155–1167, October 2013.

[21] T. Yoshikawa and O. Khatib. “Compliant Humanoid Robot Control by the Torque Transformers”. In *Proc. of the 2009 IEEE/RSJ International Conference on Intelligent Robots and Systems*, pages 3011–3018, October 2009.

[22] R. Philippsen, L. Sentis, and O. Khatib. “An Open Source Extensible Software Package to Create Whole-Body Compliant Skills in Personal Mobile Manipulators”. In *Proc. of the 2011 IEEE/RSJ International Conference on Intelligent Robots and Systems*, pages 1036–1041, September 2011.

[23] F. L. Moro, M. Gienger, A. Goswami, N. G. Tsagarakis, and D. G. Caldwell. “An Attractor-based Whole-Body Motion Control (WBMC) System for Humanoid Robots”. In *Proc. of the 13th IEEE-RAS International Conference on Humanoid Robots*, pages 42–49, October 2013.

[24] K. Nagasaka, Y. Kawanami, S. Shimizu, T. K., T. Tsuboi, A. Miyamoto, T. Fukushima, and H. Shimomura. “Whole-body Cooperative Force Control for a Two-Armed and Two-Wheeled Mobile Robot Using Generalized Inverse Dynamics and Idealized Joint Units”. In *Proc. Of the 2010 IEEE International Conference on Robotics and Automation*, pages 3377–3383, May 2010.

[25] C. Ott, B. Henze, and D. Lee. “Kinesthetic teaching of humanoid motion based on whole-body compliance control with interaction-aware balancing”. In *Proc. of the 2013 IEEE/RSJ International Conference on Intelligent Robots and Systems*, pages 4615–4621, November 2013.

[26] A. Dietrich, “Whole-Body Impedance Control of Wheeled Humanoid Robots”. Berlin, Germany: Springer, 2016.

[27] A. Heins, M. Jakob and A. P. Schoellig, "Mobile Manipulation in Unknown Environments with Differential Inverse Kinematics Control," *2021 18th Conference on Robots and Vision (CRV)*, Burnaby, BC, Canada, 2021, pp. 64-71.

[28] O. Khatib. “A Unified Approach for Motion and Force Control of Robot Manipulators: The Operational Space Formulation”. *IEEE Journal of Robotics and Automation*, RA-3(1):43–53, February 1987.

[29] M. Selvaggio, A. Garg, F. Ruggiero, G. Oriolo and B. Siciliano, "Non-Prehensile Object Transportation via Model Predictive Non-Sliding Manipulation Control," in *IEEE Transactions on Control Systems Technology*, vol. 31, no. 5, pp. 2231-2244, Sept. 2023, doi: 10.1109/TCST.2023.3277224.

[30] S. Kleff, E. Dantec, G. Saurel, N. Mansard, and L. Righetti, “Introducing force feedback in model predictive control,” in *Proc. IEEE/RSJ Int. Conf. Intell. Robots Syst.*, Oct. 2022, pp. 13379–13385.

[31] A. Gazar, G. Nava, F. J. A. Chavez and D. Pucci, "Jerk Control of Floating Base Systems With Contact-Stable Parameterized Force Feedback," in *IEEE Transactions on Robotics*, vol. 37, no. 1, pp. 1-15, Feb. 2021, doi: 10.1109/TRO.2020.3005547.

[32] A. Escande, N. Mansard, P. B. Wieber, “Hierarchical quadratic programming: Fast online humanoid-robot motion generation,” *The International Journal of Robotics Research*, SAGE Publications, 2014, 33 (7), pp.1006-1028, doi: 10.1177/0278364914521306.